catalysts

MDPI

Article

Comparison of the Photocatalytic Activity of ZnO/CeO_2 and ZnO/Yb_2O_3 Mixed Systems in the Phenol Removal from Water: A Mechanicistic Approach

Erik Cerrato, Nuno Paulo Ferreira Gonçalves, Paola Calza and Maria Cristina Paganini *

Dipartimento di Chimica e Centro NIS, via Giuria 7, 10125 Torino, Italy; erik.cerrato@unito.it (E.C.); nunopaulo.ferreiragoncalves@unito.it (N.P.F.G.); paola.calza@unito.it (P.C.)

* Correspondence: mariacristina.paganini@unito.it; Tel.: +39-011-670-7576

Received: 7 September 2020; Accepted: 14 October 2020; Published: 21 October 2020

Abstract: In this paper we compare the photocatalytic activity of two semiconductors based on ZnO: ZnO/CeO_2 and ZnO/Yb_2O_3. The two samples were prepared *via* hydrothermal synthesis and fully characterized by X-ray diffraction technique, diffuse reflectance Ultra Violet- Visible spectroscopy (UV-Vis), high resolution transmission electron microscopy and finally with electron paramagnetic resonance spectroscopy. The prepared materials were also tested in their photocatalytic performances both through Electron Paramagnetic Resonance (EPR) analyzing the formation of charge carriers and with the abatement of a probe molecule like phenol, in presence and in absence of scavengers.

Keywords: ZnO; mixed metal oxides; photocatalysts; cerium; ytterbium

1. Introduction

In recent years, many efforts have been devoted to the search for new materials that work as photocatalysts. The great interest in the catalytic processes triggered by light stems from the possibility of exploiting the cleanest and most plentiful source of energy available on earth, namely the electromagnetic radiation coming from the sun. It represents a unique and unmissable opportunity to cope with the still growing global warning and the strictly connected air pollution and water contamination [1,2]. The development of this eco-friendly technology, free from the fossil fuel, results into advanced oxidation and reductive processes able to remediate wastewaters [3,4], to generate H_2 [5–7] from water splitting and to reduce CO_2 into fuels [8,9], respectively. During the years, the materials class that has been showing the best attitude concerning the solar to chemical energy conversion has been that of transition metal oxide based semiconductors [10–12]. In general, a semiconducting material is characterized by a band structure where the electrons, located in the valence band (VB), can be photoexcited in the conduction band (CB) by the absorption of a suitable amount of energy bringing by incident light, leaving photoinduced holes in the VB [13]. Consequently, the light-promoted oxidative holes in the VB and reductive electrons in the CB give rise to the complex redox reactions at the semiconductor surface.

Historically, the first generation of semiconductor photocatalysts was essentially based on the development of the TiO_2 material [14]; it has been followed by the second-generation materials, in which TiO_2 was doped with metal and non-metals elements [15,16]. The doping procedure has been made necessary due to the fact that TiO_2 holds a band gap around 3.2 eV, falling in the UV range of the electromagnetic spectrum. As a matter of fact, the UV component of the solar radiation impinging the earth surface is just the 5%, not enough to efficiently activate TiO_2 as photocatalyst. On the other hand, the visible component hovers around the 43%; such amount prompted the scientists to sensitize the

material to visible light [1]. In practice, this can be reached by the deliberate insertion of a small amount of foreign atom inside the semiconductor lattice that could induce defect levels inside the material band gap, able to reduce the light energy needed to generate the charge carrier separation [17,18].

Currently, the third generation of photocatalysts is looking for new materials, based on metal oxides different from TiO_2, in which the constitution of interfaces and heterojunctions plays a crucial role in the photoactivity of the final products [19,20]. Among the third generation of photocatalysts, ZnO occupies a paramount role in the photocatalytic technology, being able to almost reach TiO_2 as number of dedicated papers as well as the efficiency of the photocatalytic performances [21,22]. ZnO exhibits excellent properties such as non-toxicity [23], cheapness, a high exciton binding energy of 60 meV [24,25], a high quantum yield [26], good resistance to electromagnetic radiation photocorrosion [27], a direct band gap and an optimal valence band potential, able to give rise to strong reactive oxygen species (ROS) [28]. However, the material presents some intrinsic drawbacks that have severely limited its applications in the photocatalytic field, as the UV region (3.3 eV) falling band gap and the high recombination rate [26,29]. Different types of techniques have been developed and proposed to increase the photocatalytic ability of ZnO overcoming its limitations such as the intrinsic and extrinsic doping [30–32], the formation of solid solutions and the creation of heterojunctions with other oxides [33–35]. This last strategic approach has been considered of particular importance in the developing of even more efficient transition metal oxides based photocatalysts. Indeed, the constitution of a heterojunction at the interfaces of two or more semiconductors can both help in the improvement of visible light harvesting and in the reduction of the photoexcited charge carriers' recombination rate, since they are stabilized on the two different materials [36–38]. Referring to this technology, in the recent past our and other research groups have started exploring ZnO interfaced with lanthanide oxides [39–45]. These mixed systems have shown some unpredictable and promising photocatalytic abilities that led to increasingly complex investigations aimed to shed the light and to rationalize the working mechanism at the base of the catalytic activity upon irradiation especially finalized to the mineralization of emerging pollutants. Among the tested materials, the best photocatalytic performances have been recorded for the CeO_2-ZnO and Yb_2O_3-ZnO mixed systems [40,46–50]. While for the first heterojunction system the working mechanism have been clearly understood, an undoubted interpretation still lacks for the second.

In the presented paper we propose a structural and optical comparison of the above mentioned ZnO-lanthanide oxides based heterosystems with the bare zinc oxide, with the intention to highlight the different photocatalytic activities. In addition, electron paramagnetic resonance (EPR) spectroscopy has probed the diverse photophysics of the two complex hetero-photocatalysts, confirming a promising charge carriers separation upon irradiation for the mixed systems. Still, in order to have a complete overview regarding the enhanced photocatalytic ability of the two heterojunctions (respect the bare ZnO), the photodegradation of phenol upon UV-vis irradiation has been assessed, also in presence of scavenger. The latter elucidates the fundamental role of CeO_2 and Yb_2O_3 in the improvement of the photoactivity in the corresponding mixed systems, where the solid-solid interface plays a crucial role. Finally, the strategic comparison between the novel synthetized lanthanide-based heterojunction allows us to suggest for the first time a working mechanism upon irradiation for the Yb_2O_3-ZnO mixed system.

2. Results

2.1. Structural Analysis

Figure 1 reports the X Ray Diffraction (XRD) patterns obtained for the pure ZnO and ZnO synthetized in the presence of 1 molar percentage of cerium and ytterbium, named CZ1 and YZ1, respectively. For all the three samples the diffraction pattern are characterized by the typical fingerprints of the wurtzitic hexagonal phase of ZnO (00-036-1451 ICDD (International Center for Diffraction Data) pattern) and by sharpness indicating the good degree of crystallinity [51,52]; any further reflections

have been recorded indicating the high purity of the synthetized materials. While for bare ZnO and YZ1 samples the mentioned phase is the only detected, in the case of CZ1 a further tiny reflection related to the cubic-fluorite like structure of the CeO_2 phase appears at around 2θ = 28.6°, corresponding to the (111) family planes (JCPDS (Joint Committee on Powder Diffraction Standards) NO. 34-0394), as highlighted by the zoom-in Figure 1b).

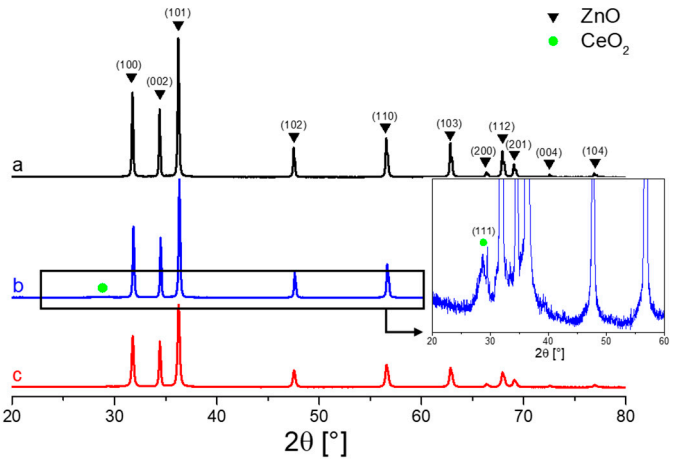

Figure 1. X-rays pattern diffraction of: (**a**) ZnO, (**b**) CZ1 and (**c**) YZ1.

The structural analysis seems suggesting a description for CZ1 sample in terms of a biphasic solid rather than a dissolution of cerium ions within the ZnO matrix. As variance, YZ1 does not show any reflection concerning Yb phases, inducing to believe in an insertion of the Yb ions inside the ZnO lattice. However, considering the different structure between the wurtzitic hexagonal phase of ZnO and the cubic phase of Y_2O_3 and the large different in the ionic radii values of 0.74 pm and 1.01 pm for Zn^{2+} and Yb^{3+}, respectively, it can be deduced that hosting Yb^{3+} ions inside ZnO structure is unlikely to achieve [33]. To further validate this hypothesis, when a dopant is inserted in the matrix of the hosted oxide it is expected a shift of some XRD reflections, indication of a drastic changing in the cell parameters of the doped material: in both cases CZ1 and YZ1 any XRD reflection shifting has been monitored concerning the ZnO wurtzitic phase. Concerning this, and as reported our previous works [45,53], the Yb related phase is of very small size and is too dispersed to be detected by XRD characterization, in contrast to the highly more aggregated CeO_2 phase.

The XRD patterns have been deeper analyzed via Rietveld refinement employed MAUD software [34] and the outcomes are reported in Table 1, where the average crystalline size (d (nm)), lattice parameters (a (Å) and c (Å)) and their difference due to the addition of lanthanide ions respect that of pure zinc oxide (Δd) are listed.

Table 1. Average crystalline size (d (nm)), lattice parameters (a (Å) and c (Å)) and their difference due to the addition of lanthanide ions respect that of pure zinc oxide (Δ*d*), Δ*a* and Δ*c* are respectively the difference between the value of *a* and *c* lattice parameter of the pure oxide(ZnO) respect to the mixed system (CZ1, YZ1).

Sample	*Phase*	*a(Å)*	*Δa*	*c(Å)*	*Δc*	*d(nm)*	*Δd*
ZnO	ZnO	3.2554	0.0000	5.2143	0.0000	256	0
CZ1	ZnO	3.2528	−0.0026	5.2111	−0.0032	163	−93
	CeO_2	5.4111				10	
YZ1	ZnO	3.2536	−0.0019	5.2122	−0.0021	93	−163

Rietveld analysis ascertains a slightest change in the lattice parameters of the zinc oxide phase for CZ1 and YZ1; however, if the lanthanide ions had entered in the zinc oxide lattice, since their

larger size respect to the zinc ion, a much greater variation in lattice parameters would have been expected. The calculated small lattice variation for the ZnO phase in the mixed systems derives by the constrain induced at the interface with the lanthanide ions. Then, also Rietveld refinement agrees with a description of biphasic solids for CZ1 and YZ1 rather than doped systems. Still in Figure 1 it is possible still to observe that the diffractograms of the mixed samples are less intense and characterized by broader reflections respect the bare ZnO pattern, implying smaller average crystal sizes for CZ1 and YZ1 than ZnO. Rietveld analysis agrees with this interpretation as noticeable in Table 1: bare ZnO shows an average size of the crystalline domain around 256 nm, CZ1 around 163 nm for the ZnO phase and 10 nm for the CeO_2 phase and, finally, YZ1 results being the smallest one, with a value of 93 nm. Thus, for CZ1 the presence of CeO_2 phase seems to limit the further growth of the ZnO phase; this intuition can be also applied for YZ1, where actually, a lower value was also found.

2.2. Optical Analysis

The DR UV-Vis spectroscopy, plotted in Figure 2, reveals that the presence of 1% of the corresponding rare earth element does not drastically affect the band gap of the mix systems CZ1 and YZ1, evaluating applying the Tauc plot method. All the characterized samples show the direct band gap transition, typical of zinc oxide with a value of 3.3 eV, due to the promotion of electrons from the valence band, mostly made up by the *2p* orbitals of O^{-2}, to the conduction band, formed by the *4s* states of Zn^{2+} [54].

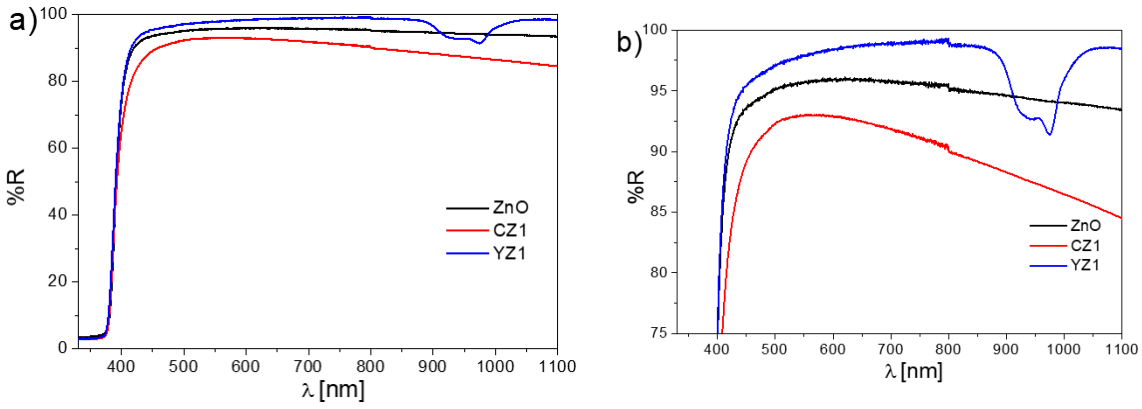

Figure 2. (**a**) Percentage of reflectance spectra of ZnO (black line), CZ1 (red line) and YZ1 (blue line); (**b**) enlargement of panel (**a**).

The fact that the mixed systems do not show a band gap shifting respect to the value of bare ZnO is a further confirmation of their very likely segregation in other phases rather than being hosted in zinc oxide lattice. Moreover, the fingerprints of Ce and Yb ions can be observed in the recorded spectra, as especially presented in Figure 2b, where an enlargement is reported. For YZ1, a broad absorption between 800 nm and 1200 nm appears, due to the Yb^{3+} f-f transitions [55–57], while for CZ1 an absorption in the visible region, around 450 nm shows up, due to the optical transition from CeO_2 valence band the empty, localized *4f* levels.

Thus, a net difference between the two lanthanide oxides present in the two mixed systems (CeO_2 for CZ1 and Yb_2O_3 for YZ1) occurs, due to the different electronic configurations: while in CeO_2, the Ce^{4+} ions shows empty 4f levels, that can accommodate electrons, for Yb_2O_3, the Yb^{3+} ions have the 4f levels fully occupied, unable to hosted electrons excited from the valence band. This variation in the electronic configuration has proved to be decisive in the working mechanism of the two mix systems upon irradiations, as discussed in the next section.

2.3. EPR Characterization

In this study, electron paramagnetic resonance (EPR) spectroscopy has been employed to monitor the presence of paramagnetic species in the synthetized samples and to follow the charge carriers' separation upon in situ irradiation, as widely discussed in our group's previous publications [16,45,58,59]. Figure 3 reports the EPR spectra of ZnO, CZ1 and YZ1 before and after the irradiation procedure under UV-vis light. The materials have been undertaken to an activation treatment before the EPR measurements as described in the **Materials and Methods** section. Pristine zinc oxide, as well as the mixed samples (black spectra in Figure 3), shows EPR signals due to paramagnetic defects also before irradiation. Despite the different attributions that it underwent in the past, it is widely accepted that the slightly symmetric line at g = 1.96 is associated with unpaired electrons in shallow donor levels or in the conduction band. The nature of the shallow donors is still cause of speculation since it has been attributed to intrinsic point defects as ionized interstitial zinc ions ($Zn_i^{\bullet}$) [60–63] or to extrinsic points defects, unintentionally inserted in the material, most probably coming from the synthesis procedure and they are: interstitial hydrogen ($H_i^{\bullet}$) [64–67] or group-III elements such as In, Al and Ga [68–72]. However, whatever the shallow donor character, the signal is found being quite independent from its nature in the published works. For this reason, nowadays, the signal is modelled as unpaired electrons bound to the defect in an effective-mass-hydrogen-like state [73]. Moving to lower magnetic field, then at higher g-value, a signal with an isotropic shape and pointed at g = 2.014 appears; also in this case the attribution has been affected by many schools of thought, but it seems to be due to the presence of ionized zinc vacancies (V_{Zn}') [74–76]. The other two g-values at $g_{\square}$ = 2.021 $g_{//}$ = 2.003 constitute the axial signal typical for O^- in ZnO [77,78]. The same description about the paramagnetic signals can be applied to the no-irradiated mixed systems, where the recorded EPR lines are due to the ZnO matrix; in addition, no paramagnetic signals due to the rare earth elements have been detected.

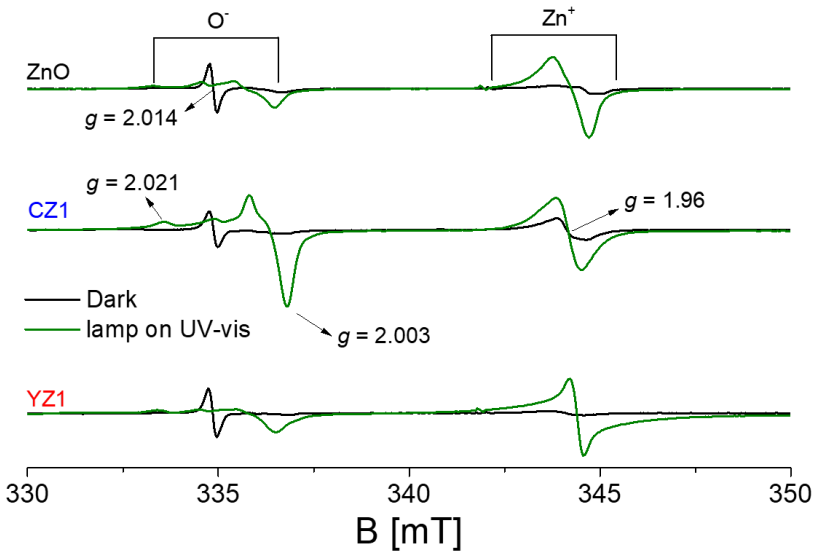

Figure 3. EPR spectra recorded ad 77 K after the activation treatment and before irradiation of ZnO, CZ1 and YZ1. Spectra in black: samples in dark. Green spectra: upon is-situ irradiation with UV-vis light at 1000 W.

Passing to the irradiated samples with UV-vis light (green spectra in Figure 3), for all the investigated samples, it is possible to observed an increase of the EPR signals associated with unpaired electrons in shallow donors (g = 1.96) and O^- species ($g_{\square}$ = 2.021 $g_{//}$ = 2.003). This phenomenon can be interpreted having in mind the band structure of a semiconductor oxide; indeed, when an electromagnetic radiation of enough energy is provided, the promotion of an electron

from the valence band to the conduction band occurs, leaving a hole in the valence band and generating a charge carriers separation. This phenomenon is described in Equation (1):

$$MeO_x + h\nu \rightarrow e^-_{(CB)} + h^+_{(VB)} \quad (1)$$

In the case that the irradiation is performed in vacuum condition, a fraction of the photoinduced charge carriers can be stabilized in the solid and detected by EPR technique, especially if the measurements are performed at 77 K (liquid nitrogen temperature) to prevent the recombination. More in detail, in semiconductor oxides, the holes are generally stabilized by oxygen ions, as described in Equation (2), causing the increase of the axial signal due to O^- ($g_\square = 2.021$ $g_{//} = 2.003$ for ZnO) [62,79,80].

$$h^+ + O_2{}^- \rightarrow O^- \quad (2)$$

On the other hand, the electrons promoted in the conduction band are stabilized in specific cations generating shallow donors, energetically meV below the conduction band, raising up the signal at $g = 1.96$. Equation (3) summarizes the occurrence. However, this description results being purely formal for ZnO, at the light of the attribution of the shallow donors nature discussed above.

$$e^- + Zn^{2+} \rightarrow Zn^+ \quad (3)$$

Summarizing, the great advantage given by EPR spectroscopy is the possibility to follow the stabilization of the photoinduced charge carriers promoted by illumination by means their stabilization inside the solid. This event causes the growth of the EPR signals related to trapped charge carriers, performing a prescreening of the material photoactivity.

Defined the signals for the detection of trapped charge carriers following irradiation, the green spectra of Figure 3, corresponding to irradiated sample in the EPR cavity at 77 K can be analyzed. It can be appreciated that the spectrum of bare ZnO as well as of the double-phase systems, show an increasing of the EPR signals related excitation and stabilization of the charge carriers as previously detailed. It is noteworthy that, from a qualitative point of view, the irradiated mixed materials display a similar behavior compared with that of bare zinc oxide, with the increase of the signals due to the stabilization of photoexcited electrons ($g = 1.96$) and holes ($g_\square = 2.021$ $g_{//} = 2.003$), where again, no signals related the lanthanides elements have been detected.

Deeper analyzing the case of the CeO_2-ZnO interface (CZ1), it emerges that the growth of the EPR signals due to the stabilization of photoinduced charge carrier is particularly evident. In case of YZ1 a smaller improvement is recorded, considering the area subdued by the EPR signal (slightly larger in case of YZ1 respect ZnO).

Hence, the constitution of the heterojunctions in the case of the mixed systems must be responsible of this enhance. Moreover, it can be observed how in the case of CZ1 the number of trapped holes is slighter higher than that of trapped electrons, revealing a different working mechanism upon visible irradiation respect to ZnO and YZ1. A further peculiarity of CZ1 sample is the fact that, while in the other two cases (ZnO and YZ1) the number of trapped holes is almost the same, the amount of photoinduced trapped holes is higher than that of photoexcited stabilized electrons. This experimental evidence reveals the working mechanism upon irradiation of the interface oxide as argued in the *discussion* section.

2.4. Photocatalytic Activity and Effect of Scavenger Addition

The photocatalytic properties resulting from the addition of ytterbium and cerium in the zinc oxide structures was investigated using phenol as a probe molecule under UVA (Ultra Violet) irradiation and results were compared with the bare ZnO. As shown in Figure 4, CZ1 and YZ1 exhibit a higher efficiency for phenol removal than the pristine material. For such, we used different scavenger aimed to elucidate the role of CeO_2 and Yb_2O_3 in the ZnO phase and consequently, in the photoreaction

processes. The phenol removal mediated by free •OH radicals (•OH_{free}) was investigated by the addition of *tert*-butanol, a selective •OH_{free} scavenger [81,82]. As shown in Figure 4, the suppression of the •OH_{free} radicals had a small inhibitory effect on phenol degradation for bare ZnO, while for CZ1 and YZ1 was observed an inhibition percentage of 52% and 34%, respectively. The role of surface adsorbed hydroxyl radicals (•OH_{ads}) in the degradation mechanism was also investigated by the addition of NaI, a well-known scavenger for holes and •OH_{ads} radicals [83–85]. Iodide ion (I^-) is an excellent scavenger that reacts with adsorbed •OH and with h^+_{vb}, as shown in the following equations:

$$I^- + h^+_{vb} \rightarrow heat \quad (4)$$

$$I^- + I^\bullet \rightarrow I_2^{\bullet -} \quad (5)$$

$$I_2^{\bullet -} \leftrightarrow I_2 + e^-_{cb} \quad (6)$$

$$I^- + {}^\bullet OH_{ads} \rightarrow I^\bullet + OH^-_{ads} \quad (7)$$

$$I^- \rightarrow I^\bullet + e^-_{cb} \quad (8)$$

In the presence of iodide, the phenol degradation rate was significantly reduced for all the materials, particularly for the doped material with an inhibition percentage >95%. The lower inhibitory effect in the presence of *tert*-butanol comparing with NaI indicate the crucial role of holes and •OH_{ads} radicals rather than •OH_{free} radicals in the photodegradation process.

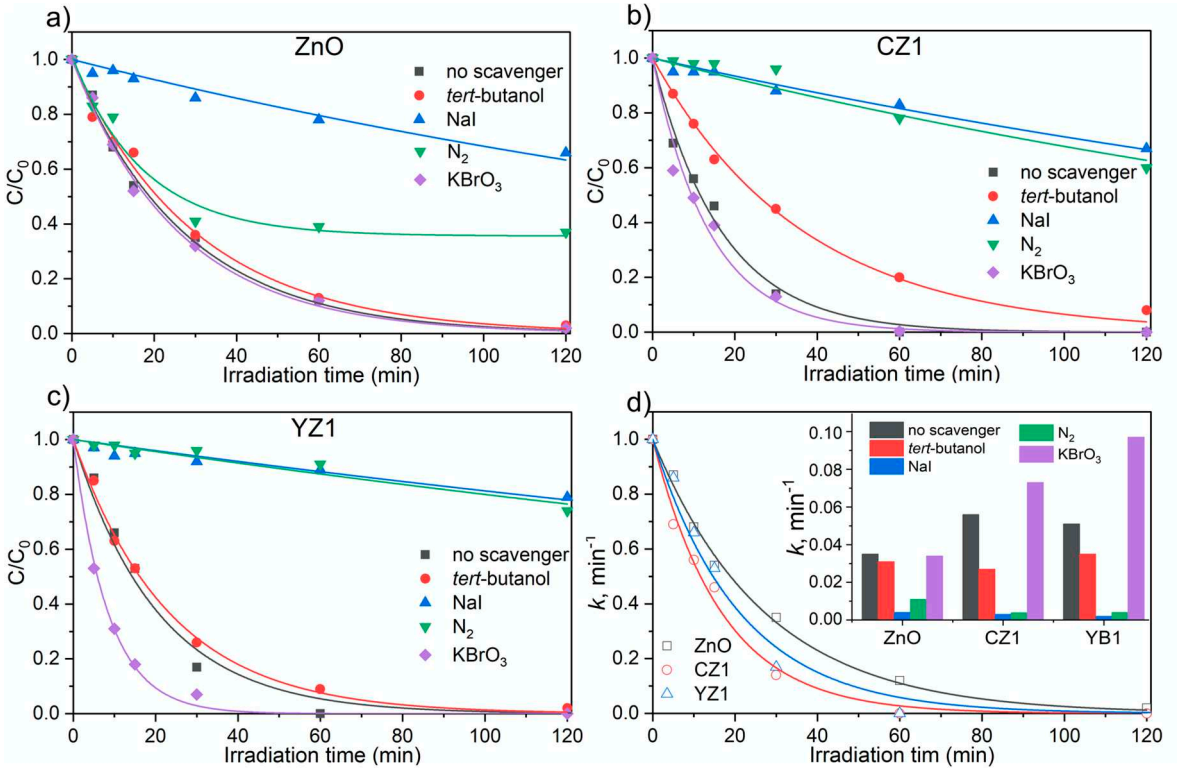

Figure 4. Photodegradation of phenol (20 mg/L) in the presence 200 mg/L of photocatalyst: (**a**) pristine ZnO; (**b**) CZ1; (**c**) YZ1 effect of addition of tert-butanol, NaI and $KBrNO_3$ (2 mM) on phenol degradation; (**d**) comparison of ZnO, CZ1 and YZ1 without scavengers. Inset: kinetics constant values.

The role of electrons in the photocatalytic process was also investigated. Molecular oxygen act as electron trap, leading to the formation of superoxide radical ion, that can form more reactive species [86], while the recombination hole/electron is prevented. The electrons mediated process was accessed performing the degradation in anoxic conditions by purging the suspension with N_2. In the

absence of oxygen, as expected, the phenol degradation rate was significantly decreased for all the photocatalysts (see Figure 4). This phenomenon is particularly distinct for CZ1 and YZ1 with a rate reduction of 93% and 96%, respectively, while for pristine ZnO the reduction was less prominent (about 70%). The addition of $KBrO_3$ as electron scavenger, [87] did not affected the performance of pristine ZnO, while for both CZ1 and YZ1 was observed a phenol removal enhancement of 30% and 83%, respectively.

3. Discussion

In this study, bare ZnO, CeO_2-ZnO (CZ1) and Yb_2O_3-ZnO (YZ1) mixed systems have been synthetized by means a hydrothermal synthetic route, characterized by an "environmentally friendly" procedure based on a green chemistry approach without the use of surfactant or organic solvents. The XRD analysis (Figure 1) have revealed high crystallinity of the synthetized samples, where the main observed phase is the one related to the wurtzitic hexagonal crystal structure of ZnO [51,52,88]; just for CZ1 a further tiny and broad reflection is discernible and imputable to the reflection of the (111) family planes of the cubic fluorite structure of CeO_2 phase. Contrary, for YZ1 XRD analysis was not able to detect an additional phase: the unique one was associated to ZnO. However, presence of Yb_2O_3 nanoparticles of rod shape, forming the Yb_2O_3-ZnO interface, has been previously detected [45,53]. Additionally, the UV-vis DR spectroscopy (Figure 2) has been able to identify the presence of Yb^{3+}, with the presence in the spectrum of YZ1 of absorptions in the NIR (Near Infra Red) region, typical of the f-f transition of Yb^{3+} [55–57]. The energy gap calculation of CZ1 and YZ1 samples attests a value of 3.3 eV as that associated to the electronic transition from the valence band to the conduction band typical of zinc oxide; then, also the UV-vis DR spectroscopy measurements seem agree with the description of the mixed materials in terms of biphasic solid than the constitution of a doped systems or solid solutions.

EPR spectroscopy has highlighted the presence in the synthetized sample of paramagnetic signals, also before that the irradiation was carried on (Figure 3), due to the trapping in the solid point defects of electrons (g = 1.96) and holes ($g_{\perp}$ = 2.021 $g_{//}$ = 2.003). Upon UV-vis irradiation, the increase of the EPR signals related trapped photogenerated charge carriers has testified the light induced activity characterizing the synthetized samples (Figure 4). In details, it has been revealed that the most active sample is CZ1 and that, in general, the constitution of the heterostructure CeO_2-ZnO brings to an improvement of the light-induced photoactivity respect the bare zinc oxide. Accordingly, with the recorded EPR spectra, it emerges that for CZ1 the number of trapped holes upon light irradiation is higher than that of trapped electrons; for the other two cases the number of trapped holes and electrons is almost the same. The presence of ceria must be responsible of this phenomenon, as already suggested by our previous works [58,89]. DFT (Density Functional Theory)calculations have verified that an electronic transition is possible from electrons photoexcited in zinc oxide conduction band to the empty, localized, *4f* levels of Ce^{4+}, that would be reduce to the paramagnetic species Ce^{3+} [58]. The experimental evidence concerning the failure to detection of the Ce^{3+} paramagnetic species lies in the nature of the rare-earth element itself: indeed, the high spin orbit constant of cerium, does not allow the observation of the Ce^{3+} EPR signal, if not at very low temperature (4 K) and hosted in octahedral symmetry of isostructural compounds [90,91], situation in which the high spin-orbit constant contribution to the spin Hamiltonian is reduced. This argumentation would explain the different number of stabilized electrons and holes during the irradiation, confirming that part of photoexcited electrons are blind to EPR technique since they are stabilized on Ce^{4+}, reduced to Ce^{3+} (then no recorded), while photoinduced holes remain stabilized on ZnO and detected as O^- ($g_{\perp}$ = 2.021 $g_{//}$ = 2.003).

Connecting the prescreening photoactivity experiments with the actual photocatalytic activity of the in-object materials, the photodegradation of phenol has been tested. Firstly, it should be noted that passing from EPR measurements to the photodegradation of the probe molecule the photoactivity

trend is maintained, where CZ1 results being the best sample in terms of charge carriers separation and photocatalytic activity, while bare ZnO is the worst.

As shown in Figure 4, the addition of charge-trapping agents (hole, electron and •OH scavengers) in the phenol photocatalytic degradation was performed to elucidate the role of CeO_2 and Yb_2O_3 phases intimately interfaced with ZnO phase. The lower inhibitory effect in the presence of *tert*-butanol ($^{\bullet}OH_{free}$ scavenger) comparing with NaI ($^{\bullet}OH_{ads}$ scavenger) indicate the crucial role of holes and $^{\bullet}OH_{ads}$ radicals rather than $^{\bullet}OH_{free}$ radicals in the photodegradation process. The higher inhibition of phenol removal suppressing the holes and free •OH observed for both, CZ1 and YZ1 suggest a higher hole production rather than ZnO, in accordance with EPR measurements upon irradiation. Nevertheless, the more significant inhibition of phenol degradation suppressing $^{\bullet}OH_{free}$ when in the presence of CZ1 indicates higher involvement of these species in the CeO_2-ZnO material. The slower phenol removal inhibition in the absence of O_2 observed for all materials evidenced the role of $e^-_{(CB)}$ on the photocatalytic process. Again, the higher $e^-_{(CB)}$ inhibition was more obvious for the CZ1 and YZ1 materials compared with the pristine ZnO. This can be attributed to the suppression of the reactive species resulting by the molecular oxygen after reacting with $e^-_{(CB)}$, however, the absence of O_2 that acts as electron trapping can promote the recombination of electron/hole. The enhancement of phenol removal when adding an external electron scavenger ($KBrO_3$) observed for CZ1, and most significantly for YZ1 can be attributed to the reaction of $e^-_{(CB)}$ with BrO_3^- [92]. Reducing in this way the electron/hole recombination and consequently increasing the availability of photogenerated holes to generate •OH. This data indicates a bigger number of photoinduced holes for CZ1 and YZ1 rather than ZnO, resulting from the incorporation of CeO_2 and Yb_2O_3 in the ZnO phase.

Ultimately, we can suggest for the first time a working mechanism also for the Yb_2O_3-ZnO heterojunction, rationalizing the outcomes arising from the photocatalytic tests in presence of electron scavengers: for YZ1 the effect of phenol removal with $KBrO_3$ is enhanced. On the base of this result, we can imagine a similar working mechanism respect to the case of CeO_2-ZnO heterostructure, inter alia the migration of the photoexcited electrons from the ZnO CB to the *4f* empty levels of cerium atoms. Analyzing in detail the chemical character of the Yb^{3+} ions of Yb_2O_3 compounds, the *4f* level are not completely empty and oppositely to cerium, they are almost full [93–95]: this situation does not favor a remarkable electronic transition. In any case, it is present as for the CeO_2-ZnO interface. Basically, less electrons are transfer to the ytterbium *4f* levels respect those transferred to the cerium *4f* levels at the heterojunction interfaces. For this reason, in presence of an electron scavenger as $KBrO_3$ the phenol removal is much more improved for YZ1 respect to that of CZ1: in YZ1 the electrons stabilized on ZnO remain in higher amount respect those in the case of CZ1. Still, this is perfectly in accordance with what emerges from the phenol photodegradation in absence of scavengers, in which definitely CZ1 exhibits the best performances.

4. Materials and Methods

4.1. Samples Preparation

The reactants employed in this work have been received by Sigma Aldrich-Merck (Rome, Italy) and used without any further purification treatment. The characterized samples have been synthetized by hydrothermal chemical route. For the bare zinc oxide sample, a solution 1M of $Zn(NO_3)_2$*$6H_2O$ has been prepared in 20 mL of deionized H_2O; then, a water solution of NaOH 4M is added dropwise until the achievement of a pH value of 11, causing the formation of a viscous suspension due to the precipitation of $Zn(OH)_2$. The obtained suspension has been transferred into a PTFE (Plytethra fluoroethylene)-lined stainless steel 100 mL autoclave and treated at 175 °C for 15 h. Finally, the product has been centrifuged and washed with deionized water. The same synthetic procedure has been employed to synthetized the mixed oxides CeO_2-ZnO (labelled CZ1) and Yb_2O_3-ZnO (labelled YZ1) adding 1% molar percentage of Ce and Yb, using $Ce(NO_3)_3$*6H2O and $Yb(NO_3)_3$*6H2O as rare earth element precursors, respectively.

4.2. Samples Characterization

The structural information of the synthetized oxides has been obtained performing X-ray Powder Diffraction (XRPD) by means a PANalytical PW3040/60 X'Pert PRO MPD, Lissone (MI) Italy (45 kV, 40 mA) with a copper K radiation source (0.15418 nm). Samples were scanned continuously in the 2θ range between 20° and 80°. The X'Pert High-Score (Malvern Panalytical Ltd, Malvern, UK) software was used to identify the mineral phases present in the samples. A Rietveld refinement was performed on the acquired patterns using the MAUD 2.2 software [8].

In order to characterize the samples from an optical point of view, Diffusive Reflectance UV-Vis spectroscopy (DRS) spectra were recorded, using a Varian Cary 5000 spectrophotometer (Agilent, CA, USA) and the Carywin-UV/scan as software (Agilent, CA, USA). A sample of PTFE with 100% reflectance was used as reference. The optical band gap energies were calculated applying the Tauc plot on the obtained spectra, considering that the energy dependence of the absorption coefficient for semiconductors in the region near the absorption edge is proportional to the material energy gap and dependent on the kind of transition (direct or indirect allowed) [9].

Electron paramagnetic resonance (EPR) spectroscopy has been employed in order to do a pre-screening of the materials photoactivity by means in-situ light irradiation through an X-band CW-EPR Bruker EMX spectrometer equipped with cylindrical cavity operating at 100 kHz field modulation (Bruker, Milan, Italy). The effect of UV and visible light on EPR spectra was investigating using a 1600W Xenon lamp (Oriel Instruments) equipped with an IR water filter (Oriel Instruments, Newport, CA, USA); during the irradiation the lamp power was set at 1000W.

4.3. Photocatalytic Degradation Experiments

The materials photocatalytic properties were investigated using phenol as a probe molecule. Experiments were performed with 200 mg/L of photocatalyst and 20 mg/L of phenol initial concentration in Pyrex glass cells filled with 5 mL volume. Samples were placed under UVA irradiation (365 nm max. emission) in a PHILIPS cleo 6× 15 W TL-D Actinic BL with irradiance from 290–400 nm and power of 90 ± 2 Wm^{-2} (CO.FO.MEGRA., Milan, Italy, power-meter). The catalyst was removed before the analysis by filtration using a 0.45 μm polyamide filter. Experiments in the absence of oxygen were performed by deaerating the suspension in the Pyrex glass cell with a continuous N_2 flow during 10 min before the irradiation. Where applicable, *tert*-butanol (2.0 mM) was added as hydroxyl scavenger, NaI (2.0 mM) as hole scavenger and $KBrO_3$ (2.0 mM) for electron scavenger were added to the photocatalytic suspension before the irradiation.

The phenol concentration over time was followed using a YL9300 HPLC system equipped with a YL9330 Column Compartment and a YL9150 autosampler and a RP C18 column (LiChroCART®, Merck, Rome, Italy, 12.5 × 0.4 cm; 5 μm) with the eluent mixture acetonitrile and phosphoric acid solution (1×10^{-2} M) at pH 2.8 (10%:90% v/v) at 1 mL/min flow rate and UV detector set at 220 nm.

5. Conclusions

In this paper we compared the photocatalytic behavior of two mixed oxides based on ZnO coupled with cerium and ytterbium oxides. These materials have been fully characterized and their photo activity have been tested with EPR technique, demonstrating that the irradiation with UV visible light brings to the formation of electrons and holes so that the charge separation occurs. Furthermore, the samples have been tested in the abatement of phenol with the presence of different scavengers for understanding the mechanism of degradation. It came out that both cerium and ytterbium oxides coupled to ZnO play an important role in the phenol abatement moreover the working mechanism is different due to the different electronic population of the two rare earth elements.

Author Contributions: Conceptualization, M.C.P. and P.C.; methodology, E.C. and N.P.F.G.; investigation, E.C.; writing—original draft preparation, E.C.; writing—review and editing, M.C.P.; supervision, M.C.P. and P.C.; project administration, M.C.P. All authors have read and agreed to the published version of the manuscript.

Funding: This research received no external funding

Acknowledgments: Financial support from the Italian MIUR through the PRIN Project 20179337R7, MULTI-e "Multielectron transfer for the conversion of small molecules: an enabling technology for the chemical use of renewable energy" and the European Union's Horizon 2020 research and innovation programme under the Marie Skłodowska-Curie Grant Agreement No 765860 (AQUAlity) are gratefully acknowledge-edged.

Conflicts of Interest: The authors declare no conflict of interest.

References

1. Lewis, N.S. Toward Cost-Effective Solar Energy Use. *Science* **2007**, *315*, 798–801. [CrossRef] [PubMed]
2. Ani, I.J.; Akpan, U.G.; Olutoye, M.A.; Hameed, B.H. Photocatalytic Degradation of Pollutants in Petroleum Refinery Wastewater by TiO_2- and ZnO-based Photocatalysts: Recent Development. *J. Clean. Prod.* **2018**, *205*, 930–954. [CrossRef]
3. Ollis, D.F.; Pelizzetti, E.; Serpone, N. Destruction of Water Contaminants. *Environ. Sci. Technol.* **1991**, *25*, 1522–1529. [CrossRef]
4. Bahnemann, D. Photocatalytic Water Treatment: Solar Energy Applications. *Sol. Energy* **2004**, *77*, 445–459. [CrossRef]
5. Tachibana, Y.; Vayssieres, L.; Durrant, J.R. Artificial Photosynthesis for Solar Water-Splitting. *Nat. Photonics* **2012**, *6*, 511–518. [CrossRef]
6. Hisatomi, T.; Kubota, J.; Domen, K. Recent Advances in Semiconductors for Photocatalytic and Photoelectrochemical Water Splitting. *Chem. Soc. Rev.* **2014**, *43*, 7520–7535. [CrossRef]
7. Domen, K.; Kondo, J.N.; Hara, M.; Takata, T. Photo- and Mechano-Catalytic Overall Water Splitting Reactions to form Hydrogen and Oxygen on Heterogeneus Catalyst. *Bull. Chem. Soc. Jpn.* **2000**, *73*, 1307–1331. [CrossRef]
8. Chang, X.; Wang, T.; Gong, J. CO_2 Photo-Reduction: Insights into CO_2 Activation and Reaction on Surfaces of Photocatalysts. *Energy Environ. Sci.* **2016**, *9*, 2177–2196. [CrossRef]
9. Vu, N.N.; Kaliaguine, S.; Do, T.O. Critical Aspects and Recent Advances in Structural Engineering of Photocatalysts for Sunlight-Driven Photocatalytic Reduction of CO_2 into Fuels. *Adv. Funct. Mater.* **2019**, *29*, 1901825. [CrossRef]
10. Zhou, P.; Yu, J.; Jaroniec, M. All-Solid-State Z-Scheme Photocatalytic Systems. *Adv. Mater.* **2014**, *26*, 4920–4935. [CrossRef]
11. Hernandez-Ramirez, A.; Medina-Ramirez, I. *Photocatalytic Semiconductors*; Springer International Publishing: Chem, Switzerland, 2015.
12. Theerthagiri, J.; Chandrasekaran, S.; Salla, S.; Elakkiya, V.; Senthil, R.A.; Nithyadharseni, P.; Maiyalagan, T.; Micheal, K.; Ayeshamariam, A.; Arasu, M.V.; et al. Recent Developments of Metal Oxide Based Heterostructures for Photocatalytic Applications Towards Environmental Remediation. *J. Solid State Chem.* **2018**, *267*, 35–52. [CrossRef]
13. Kudo, A.; Miseki, Y. Heterogeneous Photocatalyst Materials for Water Splitting. *Chem. Soc. Rev.* **2009**, *38*, 253–278. [CrossRef] [PubMed]
14. Fujishima, A.; Honda, K. Electrochemical Photolysis of Water at a Semiconductor Electrode. *Nat. Biotechnol.* **1972**, *238*, 37–38. [CrossRef]
15. Sato, S. Photocatalytic Activity of NO_X-doped TiO_2 in the Visible Light Region. *Chem. Phys. Lett.* **1986**, *123*, 126–128. [CrossRef]
16. Livraghi, S.; Paganini, M.C.; Giamello, E.; Selloni, A.; Valentin, C.D.; Pacchioni, G. Origin of Photoactivity of Nitrogen-Doped Titanium Dioxide under Visible Light. *J. Am. Chem. Soc.* **2006**, *128*, 15666–15671. [CrossRef]
17. Byrne, C.; Subramanian, G.; Pillai, S.C. Recent Advances in Photocatalysis for Environmental Applications. *J. Environ. Chem. Eng.* **2018**, *6*, 3531–3555. [CrossRef]
18. Etacheri, V.; Di Valentin, C.; Schneider, J.; Bahnemann, D.; Pillai, S.C. Visible-Light Activation of TiO_2 Photocatalysts: Advances in Theory and Experiments. *J. Photochem. Photobiol. C* **2015**, *25*, 1–29. [CrossRef]
19. Emeline, A.V.; Kuznetsov, V.N.; Ryabchuk, V.K.; Serpone, N. On the way to the creation of next generation photoactive materials. *Environ. Sci. Pollut. Res.* **2012**, *19*, 3666–3675. [CrossRef]
20. Serpone, N.; Emeline, A.V. Semiconductor Photocatalysis-Past, Present, and Future Outlook. *J. Phys. Chem. Lett.* **2012**, *3*, 673–677. [CrossRef]

21. Khan, S.T.; Malik, A. Engineered Nanomaterials for Water Decontamination and Purification: From Lab to Products. *J. Hazard. Mater.* **2019**, *363*, 295–308. [CrossRef]
22. Lee, K.M.; Lai, C.W.; Ngai, K.S.; Juan, J.C. Recent Developments of Zinc Oxide Based Photocatalyst in Water Treatment Technology: A Review. *Water Res.* **2016**, *88*, 428–448. [CrossRef]
23. Stankic, S.; Suman, S.; Haque, F.; Vidic, J. Pure and Multi Metal Oxide Nanoparticles: Synthesis, Antibacterial and Cytotoxic Properties. *J. Nanobiotechnol.* **2016**, *14*, 73. [CrossRef] [PubMed]
24. Janotti, A.; Walle, C.G.V.d. Fundamentals of Zinc Oxide as a ASemiconductor. *Rep. Prog. Phys.* **2009**, *72*, 126501–1265028. [CrossRef]
25. Reynolds, D.C.; Litton, C.W.; Collins, T.C. Zeeman Effects in the Edge Emission and Absorption of ZnO. *Phys. Rev.* **1965**, *140*, A1726–A1734. [CrossRef]
26. Özgür, Ü.; Alivov, Y.I.; Liu, C.; Teke, A.; Reshchikov, M.; Doğan, S.; Avrutin, V.; Cho, S.J.; Morkoç, H. A Comprehensive Review of ZnO Materials and Devices. *J. Appl. Phys.* **2005**, *98*, 041301–041301103. [CrossRef]
27. Rodnyi, P.A.; Khodyuk, I.V. Optical and Luminescence Properties of Zinc Oxide (Review). *Opt. Spectrosc.* **2011**, *111*, 776–785. [CrossRef]
28. Hoffmann, R.M.; Martin, S.T.; Choi, W.; Bahnemann, D.W. Environmental Applications of Semiconductor Photocatalysis. *Chem. Rev.* **1995**, *95*, 69–96. [CrossRef]
29. Klingshirn, C.; Fallert, J.; Zhou, H.; Sartor, J.; Thiele, C.; Maier-Flaig, F.; Schneider, D.; Kalt, H. 65 Cears of ZnO Research-Old and Very Recent Results. *Phys. Stat. Sol. B* **2010**, *247*, 1424–1447. [CrossRef]
30. Cerrato, E.; Paganini, M.C.; Giamello, E. Photoactivity under Visible Light of Defective ZnO Investigated by EPR Spectroscopy and Photoluminescence. *J. Photochem. Photobiol., A* **2020**, *397*, 112531. [CrossRef]
31. Medhi, R.; Marquez, M.D.; Lee, T.R. Visible-Light-Active Doped Metal Oxide Nanoparticles: Review of their Synthesis, Properties, and Applications. *ACS Appl. Nano Mater.* **2020**, *3*, 6156–6185. [CrossRef]
32. Samadi, M.; Zirak, M.; Naseri, A.; Khorashadizade, E.; Moshfegh, A.Z. Recent Progress on Doped ZnO Nanostructures for Visible-Light Photocatalysis. *Thin Solid Film.* **2016**, *605*, 2–19. [CrossRef]
33. Abebe, B.; Murthy, H.C.A.; Amare, E. Enhancing the Photocatalytic Efficiency of ZnO: Defects, Heterojunction, and Optimization. *Environ. Nanotechnol. Monit. Manag.* **2020**, *14*, 100336. [CrossRef]
34. Pirhashemi, M.; Habibi-Yangjeh, A.; Rahim Pouran, S. Review on the Criteria anticipated for the Fabrication of Highly Efficient ZnO-based Visible-Light-driven Photocatalysts. *J. Ind. Eng. Chem.* **2018**, *62*, 1–25. [CrossRef]
35. Cerrato, E.; Paganini, M.C. Mechanism of Visible Photon Absorption: Unveiling of the C_3N_4–ZnO Photoactive Interface by means of EPR Spectroscopy. *Mater. Adv.* **2020**, in press. [CrossRef]
36. Subha, N.; Mahalakshmi, M.; Myilsamy, M.; Neppolian, B.; Murugesan, V. Direct Z-scheme heterojunction nanocomposite for the enhanced solar H 2 production. *Appl. Catal. A* **2018**, *553*, 43–51. [CrossRef]
37. Xu, Q.; Zhang, L.; Yu, J.; Wageh, S.; Al-Ghamdi, A.A.; Jaroniec, M. Direct Z-Scheme Photocatalysts: Principles, Synthesis, and Applications. *Mater. Today* **2018**, *21*, 1042–1063. [CrossRef]
38. Low, J.; Yu, J.; Jaroniec, M.; Wageh, S.; Al-Ghamdi, A.A. Heterojunction Photocatalysts. *Adv. Mater.* **2017**, *29*, 16011694. [CrossRef]
39. Vaiano, V.; Matarangolo, M.; Sacco, O.; Sannino, D. Photocatalytic treatment of aqueous solutions at high dye concentration using praseodymium-doped ZnO catalysts. *Appl. Catal. B* **2017**, *209*, 621–630. [CrossRef]
40. Cerrato, E.; Gionco, C.; Berruti, I.; Sordello, F.; Calza, P.; Paganini, M.C. Rare earth ions doped ZnO: Synthesis, characterization and preliminary photoactivity assessment. *J. Solid State Chem.* **2018**, *264*, 42–47. [CrossRef]
41. Sordello, F.; Berruti, I.; Gionco, C.; Paganini, M.C.; Calza, P.; Minero, C. Photocatalytic Performances of Rare Earth Element-Doped Zinc Oxide toward Pollutant Abatement in Water and Wastewater. *Appl. Catal. B* **2019**, *245*, 159–166. [CrossRef]
42. Kumar, V.; Swart, H.C.; Gohain, M.; Kumar, V.; Som, S.; Bezuindenhoudt, B.C.B.; Ntwaeaborwa, O.M. Influence of Ultrasonication Times on the Tunable Colour Emission of ZnO Nanophosphors for Lighting Applications. *Ultrason. Sonochem.* **2014**, 1549–1556. [CrossRef] [PubMed]
43. Zamiri, R.; Lemos, A.F.; Reblo, A.; Ahangar, H.A.; Ferreira, J.M.F. Effects of Rare-Earth (Er, La and Yb) Doping on Morphology and Structure Properties of ZnO Nanostructures Prepared by Wet Chemical Method. *Ceram. Int.* **2014**, *40*, 523–529. [CrossRef]

44. Pascariu, P.; Cojocaru, C.; Olaru, N.; Samoila, P.; Airinei, A.; Ignat, M.; Sacarescu, L.; Timpu, D. Novel Rare Earth (RE-La, Er, Sm) Metal doped ZnO Photocatalysts for Degradation of Congo-Red dye: Synthesis, Characterization and Kinetic Studies. *J. Environ. Manag.* **2019**, *239*, 225–234. [CrossRef] [PubMed]
45. Cerrato, E.; Zickler, G.A.; Paganini, M.C. The Role of Yb Doped ZnO in the Charge Transfer Process and Stabilization. *J. Alloys Compd.* **2019**, *816*, 152555. [CrossRef]
46. Chouchene, B.; Ben Chaabane, T.; Balan, L.; Girot, E.; Mozet, K.; Medjahdi, G.; Schneider, R. High Performance Ce-doped ZnO Nanorods for Sunlight-Driven Photocatalysis. *Beilstein J. Nanotechnol.* **2016**, *7*, 1338–1349. [CrossRef]
47. Munawar, T.; Yasmeen, S.; Hasan, M.; Mahmood, K.; Hussain, A.; Ali, A.; Arshad, M.I.; Iqbal, F. Novel Tri-Phase Heterostructured ZnO–Yb_2O_3–Pr_2O_3 Nanocomposite; Structural, optical, Photocatalytic and Antibacterial Studies. *Ceram. Int.* **2020**, *46*, 11101–11114. [CrossRef]
48. Calza, P.; Gionco, C.; Giletta, M.; Kalaboka, M.; Sakkas, V.A.; Albanis, T.; Paganini, M.C. Assessment of the Abatement of Acelsulfame K Using Cerium Doped ZnO as Photocatalyst. *J. Hazard. Mater.* **2016**, *323*, 471–477. [CrossRef]
49. Paganini, M.C.; Dalmasso, D.; Gionco, C.; Polliotto, V.; Mantilleri, L.; Calza, P. Beyond TiO_2: Cerium-Doped Zinc Oxide as a New Photocatalyst for the Photodegradation of Persistent Pollutants. *ChemistrySelect* **2016**, *1*, 3377–3383. [CrossRef]
50. Bechambi, O.; Jlaiel, L.; Najjar, W.; Sayadi, S. Photocatalytic Degradation of Bisphenol A in the Presence of Ce-ZnO: Evolution of Kinetics, Toxicity and Photodegradation Mechanism. *Mater. Chem. Phys.* **2016**, *173*, 95–105. [CrossRef]
51. Coleman, V.A.; Jagadish, C. *Zinc Oxide Bulk, Thin Films and Nanostructures*; Pearton, S., Ed.; Elsevier: Amsterdam, The Netherlands, 2006; pp. 1–20.
52. Gerward, L.; Olsen, J.S. The High-Pressure Phase of Zincite. *J. Synchrotron Radiat.* **1995**, *2*, 233–235. [CrossRef]
53. Shestakov, M.V.; Baranov, A.N.; Tikhomirov, V.K.; Zubavichus, Y.V.; Kuznetsov, A.S.; Veligzhanin, A.A.; Kharin, A.Y.; Rösslhuber, R.; Timoshenko, V.Y.; Moshchalkov, V.V. Energy-Transfer Luminescence of a Zinc Oxide/Ytterbium Oxide Nanocomposite. *RSC Adv.* **2012**, *2*, 8783. [CrossRef]
54. Srikant, V.; Clarke, D.R. On the Optical Band Gap of Zinc Oxide. *J. Appl. Phys.* **1998**, *83*, 5447–5451. [CrossRef]
55. Reszczyńska, J.; Grzyb, T.; Sobczak, J.W.; Lisowski, W.; Gazda, M.; Ohtani, B.; Zaleska, A. Visible Light Activity of Rare Earth Metal Doped (Er3+, Yb3+ or Er3+/Yb3+) Titania Photocatalysts. *Appl. Catal. B* **2015**, *163*, 40–49. [CrossRef]
56. Carnall, W.T. *Handbook on the Physics and Chemistry of Rare Earths*; Gschneidner, K.A., Ed.; Elsevier: Amsterdam, The Netherlands, 1979; Volume 3, pp. 171–208.
57. Carnall, W.T.; Fields, P.R.; Sarup, R. Optical Absorption Spectra of Er3+:LaF3 and ErCl3 · 6H2O. *J. Chem. Phys.* **1972**, *57*, 43–51. [CrossRef]
58. Cerrato, E.; Gionco, C.; Paganini, M.C.; Giamello, E.; Albanese, E.; Pacchioni, G. Origin of Visible Light Photoactivity of the CeO_2/ZnO Heterojunction. *ACS Appl. Energy Mat.* **2018**, *1*, 4247–4260. [CrossRef]
59. Barolo, G.; Livraghi, S.; Chiesa, M.; Paganini, M.C.; Giamello, E. Mechanism of the Photoactivity under Visible Light of N-Doped Titanium Dioxide. Charge Carriers Migration in Irradiated N-TiO_2 Investigated by Electron Paramagnetic Resonance. *J. Phys. Chem. C* **2012**, *116*, 20887–20894. [CrossRef]
60. Look, D.C.; Hemsky, J.W. Residual Native Shallow Donor in ZnO. *Phys. Rev. Lett.* **1999**, *82*, 2552–2555. [CrossRef]
61. Halliburton, L.E.; Giles, N.C.; Garces, N.Y.; Luo, M.; Xu, C.; Boatner, L.B.A. Production of Native Donors in ZnO by Annealing at High Temperature in Zn Vapour. *Appl. Phys. Lett.* **2005**, *87*, 1721081–1721083. [CrossRef]
62. Wong, N.B.; Taarit, Y.B.; Lunsford, J.H. Formation of O^- in ZnO from the Dissociation of Adsorbed N_2O. *J. Chem. Phys.* **1974**, *60*, 2148–2151. [CrossRef]
63. Codell, M.; Gisser, H.; Weisberg, J.; Iyengar, R.D. Electron Spin Resonance Study of Hydroperoxide on Zinc Oxide. *J. Phys. Chem. C* **1968**, *72*, 2460–2464. [CrossRef]
64. Hofmann, D.M.; Hofstaetter, A.; Leiter, F.; Zhou, H.; Henecker, F.; Meyer, B.K.; Orlinskii, S.B.; Schmidt, J.; Baranov, P.G. Hydrogen: A Relevant Shallow Donor in Zinc Oxide. *Phys. Rev. Lett.* **2002**, *88*, 0455041–0455044. [CrossRef] [PubMed]
65. Kohan, A.F.; Ceder, G.; Morgan, D.; Van de Walle, C.G. First-Principles Study of Native Point Defects in ZnO. *Phys. Rew. B* **2000**, *61*. [CrossRef]

66. Walle, C.G.V.d. Hydrogen as a Cause of Doping in Zinc Oxide. *Phys. Rev. Lett.* **2000**, *85*, 1012–1015. [CrossRef] [PubMed]
67. Smith, J.M.; Vehse, W.E. ESR of electron irradiated ZnO confirmation of the F^+center. *Phys. Lett.* **1970**, *31A*, 147–148. [CrossRef]
68. Setaka, M.; Fujieda, S.; Kwan, T. Electron Spin Resonance of Oxidized ZnO at -195 °C. *Bull. Chem. Soc. Jpn.* **1970**, *43*, 2377–2380. [CrossRef]
69. Kokes, R.J. The influence of Chemisorption of Oxygen on the Electron Spin Resonance of zinc Oxide. *J. Phys. Chem. C* **1962**, *66*, 99–103. [CrossRef]
70. Schulz, M. ESR Experiments on Ga Donors in ZnO Crystals *Phys. Stat. Sol. A* **1975**, *27*, 5–8. [CrossRef]
71. Gonzalez, C.; Block, D.; Cox, R.T.; Hervè, A. Magnetic Resonance Studies of Shallow Donors in Zinc Oxide. *J. Cryst. Growth* **1982**, *59*, 357–362. [CrossRef]
72. Block, D.; Hervé, A.; Cox, R.T. Optically Detected Magnetic Resonance and Optically Detected ENDOR of Shallow Indium Donors in ZnO. *Phys. Rev. B* **1982**, *25*, 6049–6052. [CrossRef]
73. Meyer, B.K.; Alves, H.; Hofmann, D.M.; Kriegseis, W.; Forster, D.; Bertram, F.; Christen, J.; Hoffmann, A.; Straßburg, M.; Dworzak, M.; et al. Bound Exciton and Donor–Acceptor Pair Recombinations in ZnO. *Phys. Stat. Sol. B* **2004**, *241*, 231–260. [CrossRef]
74. Leutwein, K.; Schneider, J. Defects in Neutron-irradiated ZnO. *Z. Naturforsch.* **1971**, *26a*, 1236–1237. [CrossRef]
75. Gallad, D.; Herve, A. ESR Spectra of the Zinc Vacancy in ZnO. *Phys. Lett.* **1970**, *33A*, 1–2. [CrossRef]
76. Galland, D.; Herve, A. Temperature Ddependance of the ESR Spectrum of The Zinc Vacancy in ZnO. *Solid State Commun.* **1974**, *14*, 953–956. [CrossRef]
77. Che, M.; Tench, A.J. Characterization and Reactivity of Mononuclear Oxygen Species on Oxide Surfaces. *Adv. Catal.* **1982**, *31*.
78. Iyengar, R.D. TiO_2 and ZnO Surface Studies by Electron Spin Resonance Spectroscopy. *Adv. Colloid Interface Sci.* **1972**, *3*, 365–388. [CrossRef]
79. Volodin, A.M.; Cherkashin, A.E. ESR Studies of N_2O Interaction with Photoinduced Centers on ZnO and MgO *React. Kinet. Catal. Lett.* **1982**, *20*, 335–338. [CrossRef]
80. Volodin, A.M.; Cherkaskin, A.E. ERR Spectrum of Methyl Radicals on ZnO Surface. *React. Kinet. Catal. Lett.* **1981**, *18*, 243–246. [CrossRef]
81. Buxton, G.V.; Greenstock, C.L.; Helman, W.P.; Ross, A.B. Critical review of rate constant for reactions of hydrated electrons, hydrogen-atoms and hydroxil radicals (.OH/.O-) in aqueous-solution. *J. Phys. Chem. Ref. Data* **1988**, *17*, 513–886. [CrossRef]
82. Devi, L.G.; Kavitha, R. Enhanced photocatalytic activity of sulfur doped TiO_2 for the decomposition of phenol: A new insight into the bulk and surface modification. *Mater. Chem. Phys.* **2014**, *143*, 1300–1308. [CrossRef]
83. Kim, J.H.; Lee, H.I. Effect of surface hydroxyl groups of pure TiO_2 and modified TiO_2 on the photocatalytic oxidation of aqueous cyanide. *Korean J. Chem. Eng.* **2004**, *21*, 116–122. [CrossRef]
84. Ishibashi, K.; Fujishima, A.; Watanabe, T.; Hashimoto, K. Quantum yields of active oxidative species formed on TiO_2 photocatalyst. *J. Photochem. Photobiol. A Chem.* **2000**, *134*, 139–142. [CrossRef]
85. Palominos, R.; Freer, J.; Mondaca, M.A.; Mansilla, H.D. Evidence for hole participation during the photocatalytic oxidation of the antibiotic flumequine. *J. Photochem. Photobiol. A Chem.* **2008**, *193*, 139–145. [CrossRef]
86. Nosaka, Y.; Nosaka, A.Y. Generation and Detection of Reactive Oxygen Species in Photocatalysis. *Chem. Rev.* **2017**, *117*, 11302–11336. [CrossRef] [PubMed]
87. Kumar, S.G.; Rao, K. Zinc oxide based photocatalysis: Tailoring surface-bulk structure and related interfacial charge carrier dynamics for better environmental applications. *RSC Adv.* **2015**, *5*, 3306–3351. [CrossRef]
88. Recio, J.M.; Blanco, M.A.; Luan, V.; Pandey, R.; Gerward, L.; Olsen, J.S. Compressibility of the high-pressure rocksalt phase of ZnO. *Phys. Rev. B* **1998**, *58*, 8949–8954. [CrossRef]
89. Cerrato, E.; Gionco, C.; Paganini, M.C.; Giamello, E. Photoactivity Properties of ZnO Doped with Cerium Ions: An EPR Study. *J. Phys. Condens. Matter.* **2017**, *29*, 1–7. [CrossRef] [PubMed]
90. Schwartz, R.W.; Hill, N.J. Electron Paramagnetic Resonance Study of Ce^{3+}, Dy^{3+} and Yb^{3+} in Cs_2NaYCl_6. *J. Chem. Soc. Faraday Trans. 2* **1974**, *70*, 124–131. [CrossRef]
91. Pidol, L.; Guillot-Noël, O.; Kahn-Harari, A.; Viana, B.; Pelenc, D.; Gourier, D. EPR Study of Ce^{3+} Ions in Lutetium Silicate Scintillators $Lu_2Si_2O_7$ and Lu_2SiO_5. *J. Phys. Chem. Solids* **2006**, *67*, 643–650. [CrossRef]

92. Chen, S.F.; Liu, Y.Z. Study on the photocatalytic degradation of glyphosate by TiO_2 photocatalyst. *Chemosphere* **2007**, *67*, 1010–1017. [CrossRef]
93. Zhang, X.; Gao, S.; Gui, W.; Zeng, Q. First-Principles Study of Structure, Mechanical and Optical Properties of La- and Sc-doped Y_2O_3. *J. Rare Earths* **2019**, *37*, 879–885. [CrossRef]
94. Lòpez-Anguillar, F.; Costa-Quintana, J. A First-Principles Pseudopotential Model for the Strong Intrasite Interaction Applied to the $4f^{13}$ Configuration (Yb_2O_3). *Phys. Stat. Sol. B* **1984**, *123*, 219. [CrossRef]
95. Prokofiev, A.V.; Shelykh, A.I.; Melekh, B.T. Periodicity in the band gap variation of Ln_2X_3 (X = O, S, Se) in the lanthanide series. *J. Alloys Compd.* **1996**, *242*, 41–44. [CrossRef]